

Dynamical mechanisms underlying contrast gain control in single neurons

Yuguo Yu and Tai Sing Lee

Center for the Neural Basis of Cognition, Carnegie Mellon University, Pittsburgh, Pennsylvania 15213, USA

(Received 6 March 2003; published 8 July 2003)

Recent neurophysiological experiments have revealed that the linear and nonlinear kernels of the transfer function in sensory neurons are not static. Rather, they are adaptive to the contrast or the variance of time-varying input stimuli, exhibiting a contrast gain control phenomenon. We investigated the underlying biophysical causes of this phenomenon by simulating and analyzing the leaky integrate-and-fire and the Hodgkin-Huxley neuronal models. Our findings indicate that contrast gain control may result from the synergistic cooperation of the nonlinear dynamics of spike generation and the statistical properties of the stimuli. The resulting statistics-dependent stimulus threshold is shown to be a key factor underlying the adaptation of frequency tuning and amplitude gain of a neuron's transfer function in different stimulus environments.

DOI: 10.1103/PhysRevE.68.011901

PACS number(s): 87.10.+e, 87.80.Tq, 05.45.-a

I. INTRODUCTION

Adaptation to changes in external stimulus conditions is a ubiquitous characteristic of information processing in the nervous system [1]. Numerous experimental studies [2–13] have indicated that the amplitudes of the transfer functions of neurons in the early visual and auditory systems are not static, but depend significantly on the overall statistical properties of visual and auditory scenes. Early sensory neurons (e.g., retinal ganglion cells) have been found to be adaptive to changes in the statistics of stimuli, in terms of both the average light intensity level (see [3] for a review) and the spatial and temporal contrast or variance in light intensity (see [4] for a review). Similar adaptations to stimulus variance have been observed in other temporal parameters, such as movement velocity or intensity, in blowfly H1 neurons [5,6] and macaque V1 neurons [7], as well as in auditory neurons [8].

These phenomena are thought to be mediated by a contrast gain control mechanism [9] and serve to dynamically adjust a neuron or a neural system's output response range to match the range of its input signals, which in turn maximizes coding efficiency [10,6]. A classic example is *light adaptation*. When the mean light level is decreased, retinal ganglion cells were found to increase their sensitivity and expand their temporal integration window [1,11]. In dim or low contrast conditions, the temporal scale of the kernels was found to expand while the gain increased [12]. The dilation of the temporal kernel allows the neuron to integrate more signals before reporting to the cortex, while the increase in gain enables the neuron to process weak signals more effectively.

Much attention has been focused on the mechanisms underlying these intelligent adaptation behaviors of the nervous system, but their neural basis is not well understood at present. It is not certain whether the behavior emerges from a network interaction of neurons or is part of the intrinsic properties of an individual neuron. Biophysically, a series of recent experiments [13] and theoretical studies [14] suggested that the contrast gain control phenomenon can be found in single neurons, and the intrinsic dynamics in spike generation may play an important role.

In this paper, we applied numerical simulations and analy-

sis to the Hodgkin-Huxley (HH) [15] and leaky integrate-and-fire (LIF) neuronal models [16] to isolate and elucidate the adaptive mechanism at the level of a single neuron. We found that many of the adaptation phenomena can be found in the behavior of an individual model neuron, and that these adaptations are at least partially controlled by the basic factors related to the bifurcation dynamics of a spiking neuron. Insofar as these factors are intrinsic to neuronal spike generation, we believe that intelligent adaptation to statistical context is a fundamental and universal property of all spiking neurons in the nervous system.

II. METHODS

To investigate the adaptation of a neuron's temporal receptive field to different stimulus conditions, we used a white-noise analysis technique. This method has been used in recent neurophysiological studies for characterizing the linear and nonlinear components of the transfer functions of neurons in various physiological systems [2,17]. The specific method we used is an advanced Wiener kernel method based on the Laguerre expansion technique [18].

In this method, the discrete input-output relation of a stable nonlinear time-invariant dynamic system is decomposed into the discrete-time Volterra series [19] with finite-memory length L :

$$y(t) = h_0 + \sum_{\tau=0}^L h_1(\tau)x(t-\tau) + \sum_{\tau_1=0}^L \sum_{\tau_2=0}^L h_2(\tau_1, \tau_2) \times x(t-\tau_1)x(t-\tau_2) + \dots, \quad (1)$$

where $x(t)$ is the input data sequence, $y(t)$ is the output data sequence of the system, and t is the discrete time point in our case. Volterra kernels $\{h_0, h_1, h_2, \dots\}$ fully characterize the input-output mapping and constitute a complete and canonical representation of any stable system whose output changes infinitesimally in response to an infinitesimal change of the input signal. h_0 , the zeroth order kernel, is an offset term, usually determined by the mean value of the output. h_1 , the first order kernel, is a linear impulse response having a finite length, and higher order kernels h_j with $j \geq 2$ characterize

the nonlinearity of the system. When kernels of higher orders are incorporated, the response function of the system can be described more accurately [19].

Expansion of the Volterra kernels on a complete orthogonal Laguerre basis $b_j(t)$ transforms Eq. (1) into the multinomial expression

$$\begin{aligned} y(t) &= c_0 + \sum_{j=1}^N c_1(j)v_j(t) + \sum_{j_1=1}^N \sum_{j_2=1}^N c_2(j_1, j_2) \\ &\quad \times v_{j_1}(t)v_{j_2}(t) + \dots \\ &= f(v_1, v_2, \dots, v_j, \dots), \end{aligned} \quad (2)$$

where

$$v_j(t) = \sum_{\tau=0}^L b_j(\tau)x(t-\tau), \quad (3)$$

where $c_0, c_1(j), c_2(j_1, j_2), \dots$ represent the Laguerre expansion coefficients of the kernel $h_j(t)$ (note that $c_0 = h_0$), and $b_j(\tau)$ denotes the j th order discrete-time orthonormal Laguerre functions,

$$\begin{aligned} b_j(\tau) &= \alpha^{(\tau-j)/2} (1-\alpha)^{1/2} \sum_{k=0}^j (-1)^k \binom{\tau}{k} \binom{j}{k} \\ &\quad \times \alpha^{j-k} (1-\alpha)^k \quad (\tau \geq 0), \end{aligned} \quad (4)$$

where α ($0 < \alpha < 1$) is the Laguerre parameter that describes the asymptotic descent of the kernels $h_j(t)$ [18]. The kernel recovery was performed using the LYSIS computational package of the Biomedical Simulations Resource of the University of Southern California. In this study, we recover only the zeroth, the first, and second order kernels, i.e., $h_0, h_1,$ and h_2 , respectively.

The input signal $x(t)$ is Gaussian white noise (GWN) with a fixed, short correlation time (cut frequency = 500 Hz) with mean μ and standard deviation σ (or the noise intensity $D, 2D = \sigma^2$) as variables. The output $y(t)$ is a sequence of binary numbers corresponding to the spikes generated by the neuronal model at a resolution of 1 ms. To verify the feasibility and accuracy of the method in recovering static kernels in the appropriate parameter space, we tested the method using a model that is composed of a static linear kernel [$K_1 = \sin(\pi t/\tau_a)\exp(-t/\tau_b)$] cascaded with a static nonlinear kernel ($K_2 = K_1' \times K_1$, where K_1' is the transpose matrix of K_1).

In the simulation experiment, the model neuron is the Hodgkin-Huxley model [15], as specified below:

$$\begin{aligned} C_m \dot{V} &= -g_{\text{Na}}m^3h(V - V_{\text{Na}}) - g_{\text{K}}n^4(V - V_{\text{K}}) \\ &\quad - g_l(V - V_l) + s(t), \end{aligned} \quad (5)$$

$$\dot{m} = [m_{\infty}(V) - m]/\tau_m(V), \quad (6)$$

$$\dot{h} = [h_{\infty}(V) - h]/\tau_h(V), \quad (7)$$

$$\dot{n} = [n_{\infty}(V) - n]/\tau_n(V), \quad i = 1, \dots, N, \quad (8)$$

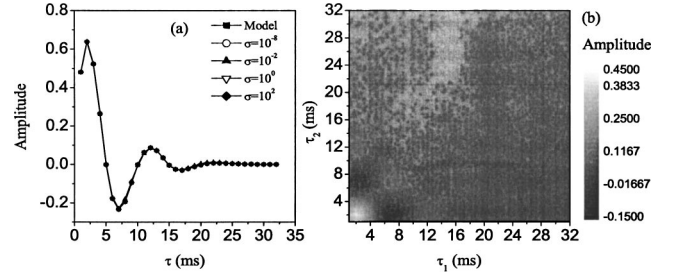


FIG. 1. (a) The first order model kernel and the recovered kernels from the method for $\sigma = 10^{-8}, 10^{-2}, 10^0,$ and 10^2 , respectively. (b) The second order kernel for $\sigma = 1$.

where V is the membrane potential and m, h and n are the gating variables of the Na^+ and K^+ channels [15], respectively. $g_{\text{Na}}, g_{\text{K}},$ and g_l are the maximal values of conductance of the sodium, potassium, and leakage currents; and $V_{\text{Na}}, V_{\text{K}},$ and V_l are the corresponding reversal potentials. The auxiliary functions and the parameter values can be found in [15]. The membrane capacity is $C_m = 1 \mu\text{F}/\text{cm}^2$. $s(t)$ is the input stimulus (GWN in our simulation) and is described as

$$s(t) = \mu + \xi(t), \quad (9)$$

$$\langle \xi(t) \rangle = 0, \quad (10)$$

$$\langle \xi(t_1)\xi(t_2) \rangle = \sigma^2 \delta(t_1 - t_2), \quad (11)$$

where μ is the mean value of the noise, σ is the standard deviation, and $\xi(t)$ is the GWN with mean zero and unit standard deviation. $\langle \dots \rangle$ represents the ensemble average over the noise distribution.

III. RESULTS

A. Identification of static kernels

First, we investigate the input parameter space in which the method works accurately and effectively. We tested the recovery of the static model kernel with noise inputs of different mean (μ) and variance (σ). This is important to establish, as otherwise it is not certain whether the change exhibited in the neuronal kernel is due to adaptation or an artifact due to the testing signals. For the static kernels (see Sec. II), we used $K_1 = \sin(\pi t/\tau_a)\exp(-t/\tau_b)$ and $K_2 = K_1' \times K_1$, with $\tau_a = \tau_b = 10$, as the first and second order kernels, respectively. The input stimulus is drawn from a Gaussian white noise distribution. We investigated the range of the standard deviation (σ) of the white noise where the method could completely and accurately recover the kernels. The recovered kernels K_1 and K_2 of the model are shown in Figs. 1(a) and 1(b). The difference between the model and the recovered kernels is estimated by a cross-correlation analysis, as shown in Fig. 2. Figure 2(a) shows that, for $\sigma \leq 10^2$, the correlation coefficient is independent of the value of σ , and approaches 1, indicating that the first order kernel can be recovered perfectly. A drop in correlation coefficient corresponds to distortion in the recovered kernel. For $\sigma > 10^2$, the correlation coefficient decreases rapidly, indicating the limitation of the

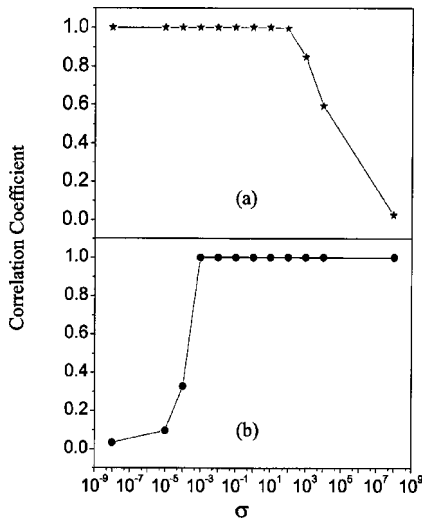


FIG. 2. The correlation coefficient between the model kernels and the recovered first order kernels (a) and second order kernels (b) as a function of σ .

method for large σ where the linear kernel is contaminated by large noise fluctuation. Therefore, we established that $\sigma \leq 10^2$ is a valid range where the kernel method can be used to recover the first order linear kernel. On the other hand, the second order kernel K_2 can be recovered perfectly when $\sigma \geq 10^{-3}$, but has problems when $\sigma < 10^{-3}$. This is because the nonlinear features of the system cannot be fully excited by a noise input with small variance.

Combining the results from Figs. 2(a) and 2(b), we conclude that the kernel recovery method can be used stably for noise with σ between 10^{-3} and 10^2 for kernels with comparable temporal scale. Within this range, the recovered kernels can be recovered accurately independent of stimuli. Outside this range, the recovered kernels contain considerable distortions. A similar conclusion is obtained for different values of τ_a and τ_b . The same results can be generated with Korenberg's fast orthogonal algorithm [20].

B. Adaptation of the kernels of the HH model

Next, using this method we investigate the adaptation of the HH model of neurons in response to different stimulus statistics. A GWN stimulus is used as input, and the resulting spike trains generated by the model are used as output. The mean of the input was fixed ($\mu=0$) and the standard deviation (σ) was varied systematically from 1 to 20 $\mu A/cm^2$. Figures 3(a) and 3(b) shows an example of an input signal (with $\sigma=3$) and the output of the HH neuron in response to it. We used 200 s of both the input and output data to recover the first and second order kernels of the HH neuron by the Laguerre expansion technique [shown in Figs. 3(c) and 3(d)].

Interestingly, we found that the kernels recovered using GWN with different values of σ are considerably different. Given that the static kernels can be recovered invariantly with these signals, the change exhibited in the kernels is indicative of the neuron's adaptation to stimulus statistics. The change is nonmonotonic: the gain amplitude of the kernel increases as σ varies from 2 to 3, but decreases when σ

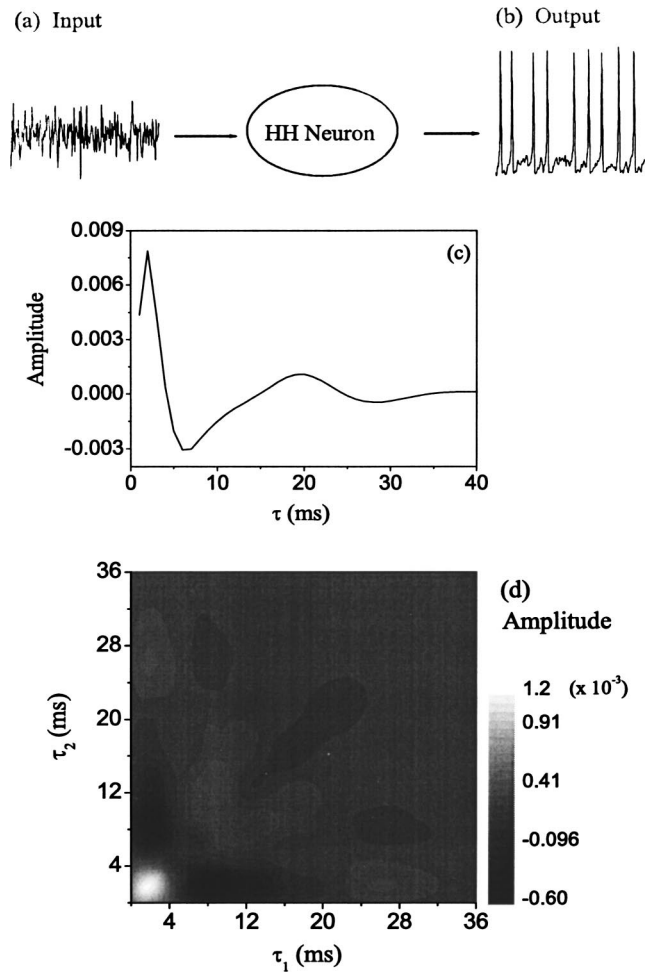


FIG. 3. Kernels of the HH neuron. (a) Input GWN signal, drawn from a normal distribution with $\mu=0$ and $\sigma=3$. (b) The spike train of the HH neuron in response to the GWN signal in (a). (c) The first order and (d) the second order kernel of the HH neuron for GWN with $\sigma=3$.

exceeds 3. Further, with an increase in σ , the kernel is found to contract in time (i.e., its peak temporal frequency increases with an increase in σ). This change in gain and temporal structure to match different noise statistics indicates that the HH neuron adapts to the statistics of the stimulus, in a similar manner to the variance or contrast adaptation observed in electrophysiological experiments [12].

To evaluate this adaptation phenomenon systematically, we computed the power spectral density (PSD) of the first order kernel recovered from stimuli generated with different σ , as shown in Fig. 4(b). For each PSD, we found that the peak frequency in the PSD (which we termed the natural frequency of the kernel) is tuned to σ . Figure 4(c) shows that the natural frequency of the kernel (f_{kernel}) increases almost linearly with an increase in σ , changing from 47 to 66 Hz as σ changes from 1 to 20. The kernel tuning frequency saturates (stops increasing) as σ exceeds 20. These findings indicate that there is a systematic relationship between the frequency tuning of a neuron and the variance of the noise stimulus input.

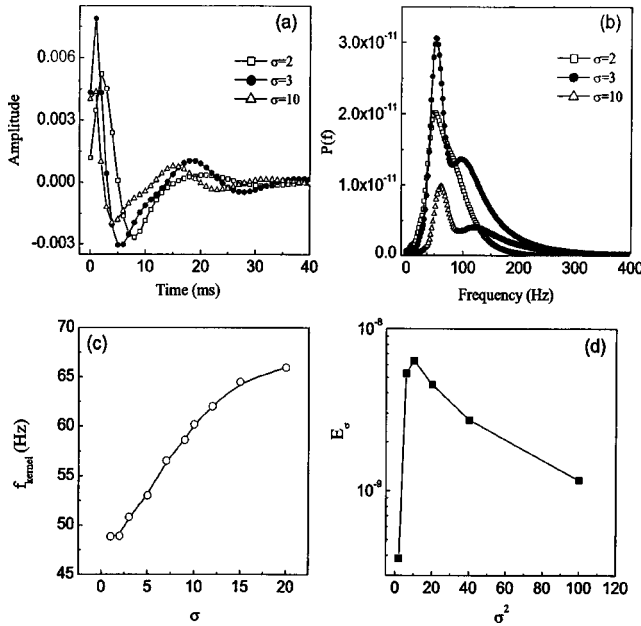


FIG. 4. Adaptation of kernels to σ . (a) The first order kernels of the HH neuron for noises with $\sigma=2,3,10$, respectively, in the case of $\mu=0$. (b) The power spectral density functions of the first order kernels for the three sets of noises. (c) The natural frequency of the first kernel as a function of σ , computed as the frequency of the maximum PSD. (d) The energy E_σ of the first order kernel as a function of σ^2 for $\mu=0$.

The PSD peak for the kernel recovered from a noise stimulus generated with $\sigma=3$ is much higher than those generated with a σ of 2 or 10. This higher gain in the PSD of the kernel allows more spectral energy to pass through for $\sigma=3$ signals. To quantify this phenomenon, we computed the total energy of the transfer function for different values of σ :

$$E = \sum_{f=0}^{F-1} [P(f)]/F, \quad (12)$$

where $P(f)$ is the power spectral density of the first or second order kernel. f is the index of frequency and F is the index of the highest frequency in the PSD. Figure 4(d) shows that E_σ first increases and then decreases with an increase in σ , reaching a maximum at $\sigma=3$. This underscores the non-monotonicity of the relation between frequency tuning and σ , demonstrating that there is a particular set of intermediate stimulus statistics that can drive the neuron in the maximally sensitive state.

Next, we investigate the sensitivity of this adaptation to the mean of the input noise signals. Figure 5(a) shows the energy of the first order kernel (i.e., E_σ as a function of σ for μ ranges from 0 to 8). We found that there exists a critical value $\mu_c \approx 6.2$, below which E_σ shows a global maximum at an intermediate σ , and above which E_σ decreases logarithmically with an increase in σ_2 . The same phenomenon is observed also in the second order kernel [Fig. 5(c)]. This critical μ_c is the stimulus current threshold for generating a spike, corresponding to the HH neuron's saddle-node bifurcation point [21]. Figures 5(b) and 5(d) show how E of the

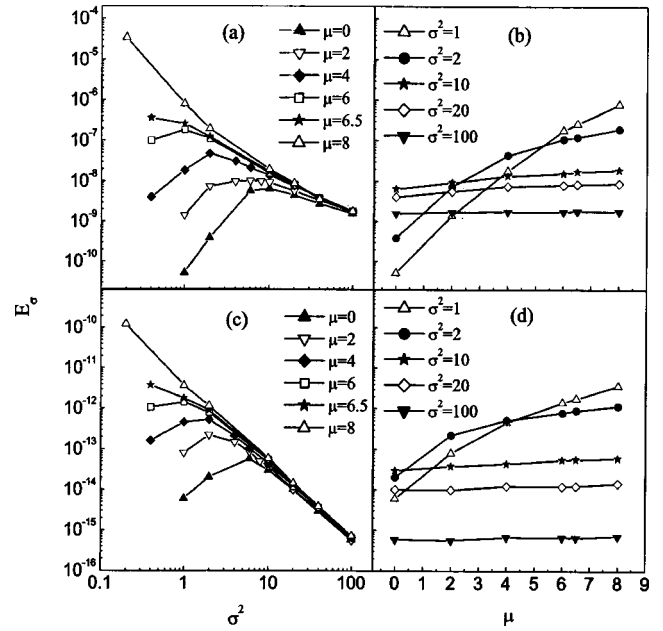


FIG. 5. The energy E_σ of the first order kernel as a function of (a) σ^2 for different values of μ and (b) μ for different values of σ^2 . The energy E_σ of the second order kernel as a function of (c) σ^2 for different values of μ and (d) μ for different values of σ^2 .

first and second order kernels change with μ for different fixed σ_2 . It can be observed that for small σ E increases rapidly with μ , while for larger σ E increases very slowly. This suggests that, when the input variance is small, the neuron is sensitive to the stimulus, but as the input variance increases, it loses its stimulus sensitivity and is controlled instead by the stochasticity of the stimulus.

The above results demonstrate that the linear kernel h_1 and the nonlinear kernel h_2 are adaptive and tuned to statistics (σ and μ) of the stimulus. The neuron exhibits tuning to σ , and this tuning is controlled by the value of μ in its relation to the stimulus current threshold (μ_c). This indicates that the adaptation phenomenon is intimately connected to the bifurcation dynamics in spike generation, which we will investigate further through analytical methods in the next section.

C. Analytical results based on LIF model

The above simulation results suggest that the contrast gain control observed in neurophysiological experiments might originate from the basic dynamical mechanism underlying spike generation. To investigate the critical determining factors in the spike generation dynamics that contribute to adaptation, we analyzed the simplest neuronal model, called the leaky integrate-and-fire model. The HH neuron model is characterized by many variables and complex dynamics, making it difficult to isolate the essential features. The LIF model captures two main properties of an excitable neuron: all-or-none firing behavior related to bifurcation, and a refractory period during which the neuron recovers its excitability. We seek to understand which of these features are key to the adaptation phenomenon. The LIF model is similar to a RC circuit in physics and is given by

$$dV/dt = -V/\tau_m + \mu + \sigma\xi(t) \quad \text{if } V(t) < V_{\text{th}}, \quad (13)$$

$$V(t^+) = V_0 \quad \text{if } V(t^-) = V_{\text{th}}, \quad (14)$$

where $\tau_m = RC$ is the time constant of the neuron with resistance R and capacitance C . Here, $V_0 = 0$ mV, $V_{\text{th}} = 12$ mV, $\tau_m = 10$ ms, $R = 3$ M Ω , $C = 3.33$ nF, and the absolute refractory period $\tau_{\text{ref}} = 4$ ms. μ is the mean value of the Gaussian white noise.

We derive below the input-output relationship of the neuron as a function of σ and μ and examine how the sensitivity of the neuron changes as a function of σ and μ . The linear part of the model [Eq. (13)] combines with the nonlinear part [Eq. (14)] to create a saddle-node bifurcation point at μ_c . When $\sigma = 0$, the membrane potential $V(t)$ relaxes to a stable equilibrium [i.e., the resting state $\mu\tau$ [16] for subthreshold stimulus ($\mu < \mu_c = V_{\text{th}}/R$)]. When $\mu \geq \mu_c$, the membrane potential will cross the threshold, generating a spike. For a GWN input stimulus with $\sigma \neq 0$, the evolution of the probability distribution of the membrane potential V is given by a well-known stochastic diffusion process, also called the Ornstein-Uhlenbeck process given by Eq. (15), which is a type of transformed Brownian motion process. The probability distribution of a neuron's voltage potential V at time t is given by a probability density function $P(V, t)$ that satisfies the Fokker-Planck equation [16,22]:

$$\frac{\partial P(V, t)}{\partial t} = \frac{1}{2} \sigma^2 \frac{\partial^2 P(V, t)}{\partial V^2} - \frac{\partial}{\partial V} \left[\left(\mu - \frac{V}{\tau_m} \right) P(V, t) \right], \quad (15)$$

with an absorbing boundary condition $P(V_{\text{th}}, t) = 0$ [22] and satisfying the following normalization:

$$\int_{-\infty}^{V_{\text{th}}} P(V, t) dV = 1. \quad (16)$$

In stationary conditions, the mean firing spike rate (r), or the flux of realizations crossing the threshold, is given by the flux

$$r = \left[\left(\mu - \frac{V}{\tau_m} \right) P(V, t) - \frac{1}{2} \sigma^2 \frac{\partial P(V, t)}{\partial V} \right]_{V_{\text{th}}} = - \frac{1}{2} \sigma^2 \frac{\partial P}{\partial V} \Big|_{V_{\text{th}}}. \quad (17)$$

The time-independent stationary firing rate r can then be derived from the above equations as [16,22]

$$r = 1 \left/ \left(\tau_{\text{ref}} + \sqrt{\pi} \tau_m \int_a^b \exp(x^2) [1 - \text{erf}(x)] dx \right), \quad (18)$$

with $a = \tau_m(\mu - V_{\text{th}}/R)/\sigma\sqrt{\tau_m}$ and $b = \tau_m\mu/\sigma\sqrt{\tau_m}$, where r , τ_{ref} , and τ_m are the mean firing rate, the absolute refractory period, and the membrane time constant of the neuron, re-

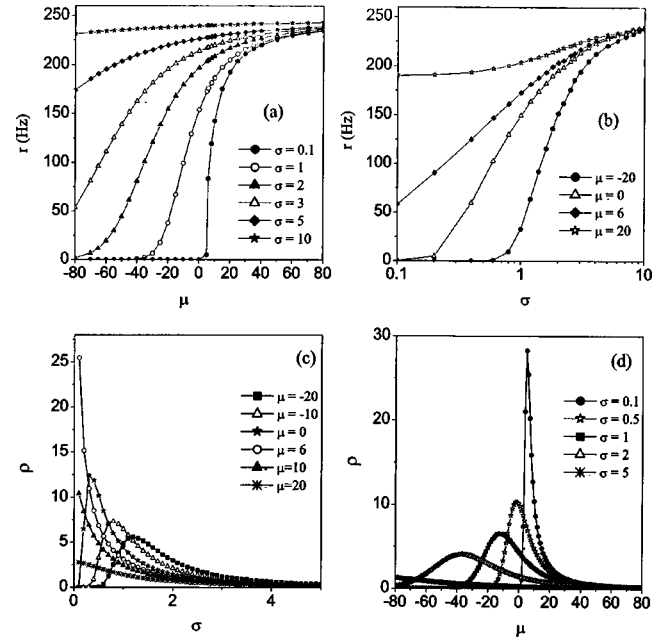


FIG. 6. The mean firing rate as a function of (a) μ for various σ and (b) σ for various μ . The static incremental sensitivity ρ represented by the integral of the first order kernel, as a function of (c) σ for various μ and (d) μ for various σ .

spectively. $\text{erf}(x)$ is the error function. The analytical input-output relations of r as a function of μ and σ are plotted in Figs. 6(a) and 6(b). Figure 6(a) shows that the firing rate r increases roughly sigmoidally with μ for small σ , but linearly with μ for larger σ .

The critical point where $r \geq 0$, at which the neuron starts to fire, shifts to the left as σ increases (i.e., the bifurcation point has moved to the left), suggesting that the neuron becomes more sensitive to the lower mean current input. The shifting of the bifurcation point induced by noise may be a critical factor underlying kernel adaptation in a neuron. In addition, we observe that the slope of the $r \sim \mu$ curve is sharper for small σ and decreases with an increase in σ . This indicates that the neuron is more sensitive to a change in weak stimulus in low signal variance than in high signal variance, corresponding to a change in sensitivity in the transfer function as a function of σ . The flattening of the slope with a high value of σ also means that the exact location of the bifurcation point has become ambiguous, implying that the neuron's spike generation might become more stochastic. Figure 6(b) provides another view of the data in Fig. 6(a). It shows the dependency of the firing rate on σ at different fixed values of μ . For all values of μ , the firing rate (r) first increases with σ and then saturates at large values of σ , exhibiting a tuning to both σ and μ .

To investigate how the sensitivity slope of the input-output relationship (transfer function) changes with the statistical parameters, we perform the following analysis. First, we linearly approximate the input-output relationship and write the input signal $s(t)$ and output mean firing rate $r(t)$ of the neuron as

$$r(s_0 + \delta s) = r_0(s_0) + \delta s \int_0^\infty h(\tau; s_0) d\tau, \quad (19)$$

where h is the first order kernel. The local slope ρ of the input-output curve, which is called the static incremental sensitivity [23], can be shown to be the integral of the first order kernel,

$$\rho = \frac{dr}{d\mu} = \int_0^\infty h(\tau; \mu) d\tau. \quad (20)$$

Combining Eqs. (18) and (20), we can express the incremental sensitivity in terms of σ and μ . The results are plotted in Figs. 6(c) and 6(d). Figure 6(c) shows that, for $\mu < \mu_c = 6$, the incremental sensitivity shows a global maximum at an intermediate σ . The exact σ for the maximum is a function of μ . For $\mu \geq \mu_c = 6$, the incremental sensitivity decreases monotonically as a function of σ . $\mu_c = 6$ serves as a boundary that divides the system's behaviors into two different dynamical regimes, comparable to the dependency of the kernel gain energy of the HH model as a function of σ and μ as shown in Fig. 5(a).

Figure 6(d) shows the relationships between incremental sensitivity ρ and μ for different values of σ . For small σ (e.g., $\sigma = 0.1$), the sensitivity curve shows a very sharp peak near the current threshold (bifurcation point), $\mu_c = 6$. As σ increases, the corresponding peak shifts to the left and becomes more smooth. This implies that for stimuli with large variance the bifurcation point of the system shifts left and becomes more ambiguous, consistent with what we saw in Fig. 6(a). The decrease of the current threshold makes the neuron more sensitive to the input signal, while the ambiguity in its location introduces randomness in spike generation. Therefore, there is a trade-off between an increase in sensitivity and an increase in randomness. There exists a value of σ at which this trade-off is maximum in signal to noise ratio, i.e., where the neuron is most sensitive to the input signal in the context of noise. Thus, a certain level of variance in the stimulus input is most synergistic with the nonlinear threshold dynamics of the neuron, driving the neuron to fire more quasiregularly, resulting in a maximal gain in transfer function. That is the underlying reason for the contrast or variance tuning phenomenon. The change in gain amplitude of the kernels in experiments is a result of the shift in the effective bifurcation point of the system induced by variations in the stimulus. We have experimented with a variety of values of the LIF model parameters, such as $\tau_m = RC$, v_{th} , and we found that, while the peak location and the curve shape can change quantitatively with these parameters, the basic adaptation phenomenon is qualitatively similar to what we have shown here.

The incremental sensitivity maximized at an intermediate σ [Fig. 6(c)] in the σ -tuning curve is of significance because it suggests that the nonlinear dynamics of a neuron resonate with a particular set of stimulus statistics. This might allow it to encode the stimulus of its preferred statistics with maximum efficiency. The synergistic cooperation between the signal variance and the neuron's dynamics allows the neuron to absorb the energy of the stimulus environment and to process

some preferred information with maximum efficiency. A population of neurons tuned to different values of σ might provide an optimal coverage to the stimulus space. This σ -dependent resonance is consistent with the earlier observed phenomena in many nonlinear systems, i.e., stochastic resonance (SR) [24] and coherence resonance (CR) [25]. A common feature of SR and CR is that the coherence measure or signal to noise ratio in the output of a nonlinear threshold system can be maximized by the additional noise with the optimal noise variance. Work on this issue has implicated the threshold condition in nonlinear system as the key underlying factor [24,25]. Thus, our results show that threshold bifurcation dynamics is likely the key factor underlying neuronal adaptation.

IV. DISCUSSION AND CONCLUSION

Adaptation to the statistics of the stimulus has been observed in many sensory systems. The global statistics of the stimulus appear to play an important role in modifying the transfer function of the neuron to optimize information encoding [26]. The transfer function of a neuron, sometimes called the receptive field in sensory systems, is therefore not simply a property of the neuron alone, but rather an emergent property that arises from synergistic interaction between the neuron and its sensory environment [27].

In this paper, we applied system identification techniques to study the kernel adaptation of the HH model and performed a theoretical analysis on the LIF model to investigate the possible dynamical origin of neuronal adaptation. We found that the amplitude and energy of the linear and nonlinear kernels of the neuronal model can change according to the statistics of the input stimuli, displaying a statistics-dependent gain control phenomenon. In particular, for mean values of the stimulus less than the stimulus threshold (μ_c), the transfer function exhibits maximum gain at some intermediate stimulus variance, showing a tuning to stimulus variance. The time scale of the model kernel contracts with an increase in μ or σ , consistent with experimental observations in variance adaptation [9,12]. These findings suggest that the variance adaptation observed originates from the nonlinear threshold dynamics of spike generation. Analysis of a LIF model reveals that the change of effective stimulus threshold in various statistical stimulus environments is the key factor underlying variance or contrast gain control. Recent experiments [13] on cortical neurons strongly supported this conclusion, finding that the gain modulation commonly seen *in vivo* may arise from varying levels of background synaptic noisy input.

Given that the LIF model captures the basic features of almost all excitable neurons, our results suggest that variance or contrast gain control might be a universal mechanism embodied in all spiking neurons for maximizing information encoding and transmission. When neurons are embedded in a network, a more sophisticated intelligent adaptation might emerge to optimize the function of the neural system. The findings provided in this paper reveal that the basic mechanism of contrast gain control is already embodied in a single neuron.

ACKNOWLEDGMENTS

We would like to thank Dr. Stelios Smirnakis, Dr. Michael E. Rudd, Dr. Carson Chow, and Dr. Matthew A. Smith for

helpful discussions. This research is supported by NSF Grant No. CAREER 9984706, NIH Vision Research Core Grant No. EY08098, and a NIH Grant No. 2P41PR06009-11 for biomedical supercomputing.

-
- [1] H. B. Barlow, R. Fitzhugh, and S. W. Kuffler, *J. Physiol. (London)* **137**, 338 (1957); S. A. Baccus and M. Meister, *Neuron* **36**, 909 (2002).
- [2] M. J. Korenberg, in *Proceedings of the 10th Annual Rocky Mountain Bioengineering Symposium*, edited by M. J. Korenberg (IEEE, New York, 1973), p. 47; P. Z. Marmarelis and V. Z. Marmarelis, *Analysis of Physiological Systems: The White-Noise Approach* (Plenum, New York, 1978); H. M. Sakai, *Physiol. Rev.* **72**, 491 (1992).
- [3] J. Walraven, C. Enroth-Cugell, D. C. Hood, D. I. A. MacLeod, and J. L. Schnapf, in *Visual Perception: The Neurophysiological Foundations*, edited by L. Spillmann and S. J. Werner (Academic, San Diego, 1990), pp. 53–101.
- [4] R. Shapley, *Curr. Biol.* **7**, 421 (1997); M. Meister and M. J. Berry, *Neuron* **22**, 435 (1999).
- [5] S. B. Laughlin, in *Handbook of Sensory Physiology*, edited by H. Autrum (Springer, Berlin, 1981), Vol. 7 (6B), pp. 133–280; R. R. de Ruyter van Steveninck, W. H. Zaagman, and H. A. K. Mastebroek, *Biol. Cybern.* **54**, 223 (1986); R. R. de Ruyter van Steveninck, W. Bialek, M. Potters, R. H. Carlson, and G. D. Lewen, in *Natural and Artificial Parallel Computation, Proceedings of the Fifth NEC Research Symposium*, edited by D. L. Waltz (SIAM, Philadelphia, 1996), pp. 21–41.
- [6] N. Brenner, W. Bialek, and R. R. de Ruyter van Steveninck, *Neuron* **26**, 695 (2000); A. L. Fairhall, G. D. Lewen, W. Bialek, and R. R. de Ruyter van Steveninck, *Nature (London)* **412**, 787 (2001).
- [7] R. D. Romero, Y. Yu, P. Afshar, and T. S. Lee, *Neurocomputing* **52–54**, 135 (2003).
- [8] R. L. Jenison, J. W. H. Schnupp, R. A. Reale, and J. F. Brugge, *J. Neurosci.* **21**, 4408 (2001).
- [9] R. M. Shapley and J. D. Victor, *Vision Res.* **19**, 431 (1979); *J. Physiol. (London)* **290**, 141 (1979); **302**, 535 (1980).
- [10] M. J. Wainwright, *Vision Res.* **39**, 3960 (1999).
- [11] R. Shapley and C. Enroth-Cugell, *Prog. Retinal Res.* **3**, 263 (1984).
- [12] H. M. Sakai and K.-I. Naka, *J. Gen. Physiol.* **105**, 815 (1995); S. M. Smirnakis, M. J. Berry, D. K. Warland, W. Bialek, and M. Meister, *Nature (London)* **386**, 69 (1997); E. A. Benardete and E. Kaplan, *Visual Neurosci.* **16**, 355 (1999); S. P. Brown and R. H. Masland, *Nat. Neurosci.* **4**, 44 (2001); K. J. Kim and F. Rieke, *J. Neurosci.* **21**, 287 (2001); D. Chander and E. J. Chichilnisky, *ibid.* **21**, 9904 (2001).
- [13] F. S. Chance, L. F. Abbott, and A. D. Reyes, *Neuron* **35**, 773 (2001); M. V. Sanchez-Vives, L. G. Nowak, and D. A. McCormick, *J. Neurosci.* **20**, 4286 (2000); **20**, 4267 (2000).
- [14] M. E. Rudd and L. Brown, *Neural Comput.* **9**, 1047 (1997); Y. G. Yu and T. S. Lee, *Neurocomputing* **52–54**, 441 (2003); L. Paninski, B. Lau, and A. Reyes, *ibid.* **52–54**, 877 (2003); J. W. Pillow and E. P. Simoncelli, *ibid.* **52–54**, 109 (2003).
- [15] A. L. Hodgkin and A. F. Huxley, *J. Physiol. (London)* **117**, 500 (1952).
- [16] L. M. Ricciardi, *Diffusion Processes and Related Topics on Biology* (Springer-Verlag, Berlin, 1977).
- [17] Y. W. Lee and M. Schetzen, *Nit. J. Control.* **2**, 237 (1965).
- [18] V. Z. Marmarelis, *Ann. Biomed. Eng.* **21**, 573 (1993).
- [19] A. Volterra, *Theory of Functions and of Integral and Integro-Differential Equations* (Dover, New York, 1930).
- [20] M. J. Korenberg, *Ann. Biomed. Eng.* **16**, 123 (1988).
- [21] H. R. Wilson, *Spikes, Decisions, and Actions: The Dynamical Foundations of Neuroscience* (Oxford University Press, New York, 1999).
- [22] N. Brunel, *J. Comput. Neurosci.* **8**, 183 (2000).
- [23] T. Hida, *Advanced Mathematical Approach to Biology* (World Scientific, Singapore, 1997).
- [24] L. Gammitoni, P. Hänggi, P. Jung, and F. Marchesoni, *Rev. Mod. Phys.* **70**, 223 (1998).
- [25] G. Hu, T. Ditzinger, C. Bing, and H. Haken, *Phys. Rev. Lett.* **71**, 807 (1993); A. S. Pikovsky and J. Kurths, *ibid.* **78**, 775 (1997).
- [26] Z. F. Mainen and T. J. Sejnowski, *Science* **268**, 1503 (1995).
- [27] W. Bialek and A. Zee, *J. Stat. Phys.* **59**, 103 (1990); F. Rieke, D. Warland, R. R. de Ruyter van Steveninck, and W. Bialek, *Spikes: Exploring the Neural Code* (MIT Press, Cambridge, MA, 1997).